

Chapter 2

Conventional Thermal Processes

Hisham Ettouney

Abstract Thermal desalination processes account for about 50% of the entire desalination market. The remaining market share is dominated by the reverse osmosis (RO) process. The main thermal desalination processes include multi-stage flash desalination (MSF), multiple-effect distillation (MED), and mechanical vapor compression (MVC). Other thermal desalination processes, e.g., solar stills, humidification dehumidification, freezing, etc., are only found on a pilot or experimental scale. Thermal desalination processes consume a larger amount of energy than RO; approximately the equivalent of 10–15 kWh/m³ for thermal processes versus 5 kWh/m³ for RO. Irrespective of this, the reliability and massive field experience in thermal desalination keeps its production cost competitive compared to the RO process. Also, the large scale production capacity for a single MSF unit, approximately 75,000 m³/day, is sufficient to provide potable water for 300,000 inhabitants. An increase in production capacity for the MED system has been realised recently, with unit production capacities of up to 30,000 m³/day. This chapter covers various aspects of thermal desalination processes. It includes a review of design, operating, and performance parameters. The analysis for each process includes a brief review of some of the recent literature studies, process descriptions, process models, and an illustration of system design and performance analysis. The chapter is divided into two parts, the first is on evaporation processes, which includes MED and MVC, and the second is on flashing processes, which include MSF. Each section starts with a description and analysis of the individual stage, for either evaporation or flashing. This is to simplify the explanation of the main processes that takes place during evaporation or flashing. Each division gives a complete description of each desalination process, together with the main modelling equations. Performance charts are presented for each system and explained in terms of main design and operating conditions.

H. Ettouney (✉)

Department of Chemical Engineering, College of Engineering and Petroleum, Kuwait University,
P.O. Box 5969 – Safat 13060, Kuwait
e-mail: ettouney@hotmail.com

2.1 Conventional Thermal Desalination Processes

Multi-stage flash (MSF), multiple-effect distillation (MED) and mechanical vapour compression (MVC) are the main thermal desalination processes. The market shares of these three processes are 87.3, 12.5, and 0.2% for MSF, MED and MVC, respectively [1]. Other types of thermal desalination processes, i.e. solar stills, humidification-dehumidification and freezing, are not found on a commercial scale and are limited to either experimental types or conceptual designs [2].

MSF and MED systems are often constructed in cogeneration plants where power and water are produced simultaneously. This is convenient because both systems require low pressure heating steam which can be easily extracted from the power plant at fairly low cost. The MVC system is operated solely on electric power.

The material presented in this chapter focuses on description, modelling and analysis of the main desalination processes. The discussion starts by explaining the elements of the evaporation and flashing processes. This is followed by a description of the entire flow diagram for each of the three processes. The main performance charts are presented for each process. Discussion of the evaporation systems includes multiple effect distillation combined with thermal and mechanical vapour compression, as well as single effect mechanical vapour compression. The section on the MSF process includes a description of the flashing stage elements, as well as a description and modelling of the MSF process.

2.2 Evaporators

Thermal evaporation is the principal mechanism in generating fresh water vapour from seawater. The evaporation process is based on creating a hot surface using heating steam; the heating steam condenses on one side and vapour is formed on the other. Evaporators include submerged tube, falling films and plates [3].

Figure 2.1 shows a schematic of a two-effect submerged tube evaporator. As shown, heating steam condenses on the wall of the tube in the first effect, and releases its latent heat to a thin layer of liquid surrounding the outside surfaces of the tubes. This results in the formation and release of vapour bubbles, which rise through the liquid and are released into the vapour space. The formed vapour is routed to the second effect, where it condenses on the wall of the tube and results in the formation of a smaller quantity of vapour. The vapour released in the second effect can be either routed to another effect, or condensed against the feed seawater.

Submerged tube evaporators are used in household humidifiers and electric kettles. They were also used in small industrial desalination units during the first half of the twentieth century. These early units were plagued with rapid fouling and scaling of the outside surface of the tubes. This required lengthy and expensive cleaning procedures of the tube bundle.

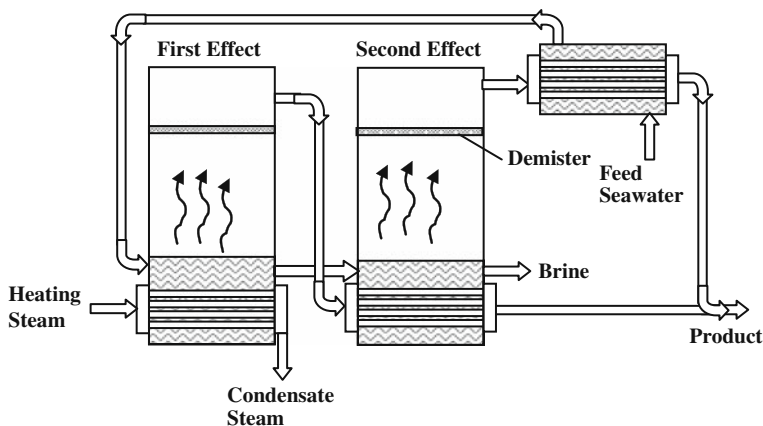


Fig. 2.1 Elements of two-effect submerged evaporator

Another drawback of the submerged tube evaporator is the reduction in the overall heat transfer coefficient, caused by the static head of liquid surrounding the outside surface of the tube. This hinders the formation, growth and release of vapour bubbles.

The falling film configuration eliminates the drawbacks of the submerged tube evaporator [4]. As shown in Figs. 2.2 and 2.3, there are two arrangements for the falling film system which include horizontal or vertical tubes. The horizontal falling film evaporator (Fig. 2.2) eliminates the static pressure effect on the evaporating surface, and as a result, higher overall heat transfer coefficients are obtained. However, the horizontal falling film arrangement necessitates operation at temperatures below 70°C , to limit the scaling rate of the outside surface of the tubes and to reduce the frequency of chemical cleaning. The horizontal falling film configuration is the industry standard and is used in most MED and MVC systems.

Figure 2.3 shows a schematic of a vertical tube falling film evaporator. As shown, the feed seawater forms a thin falling film on the inside surfaces of the tubes. Film formation is more difficult to maintain and control than with horizontal falling film. As a result, dry patches may form and result in a high scaling rate and uneven tube expansion. Although the vertical tube arrangement allows for use of on-line ball

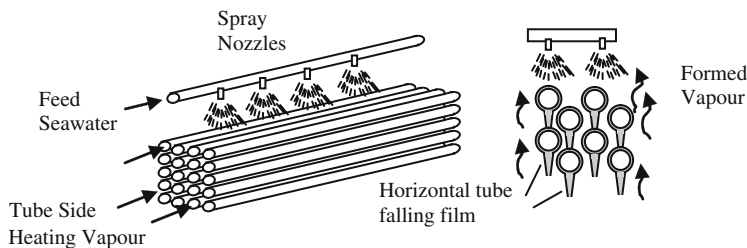
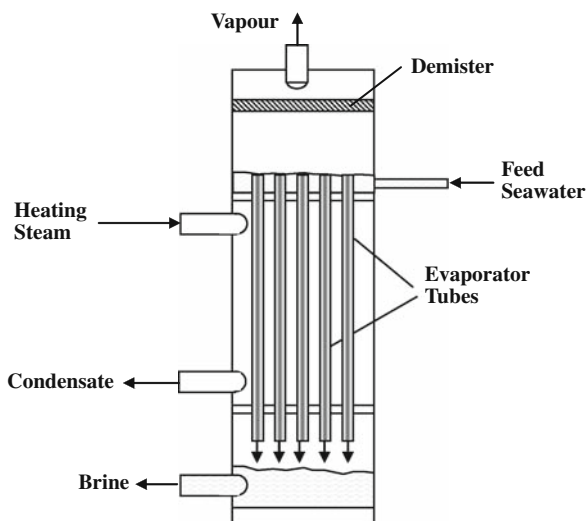


Fig. 2.2 Horizontal tube falling film evaporator

Fig. 2.3 Vertical tube falling film evaporator



cleaning, which would considerably reduce the scaling effects and allow for higher temperature operation, it is used on a very limited scale in the desalination industry.

Plate evaporators have been developed and tested on limited scale [5]. A schematic for the plate evaporator is shown in Fig. 2.4, where the heating steam condenses on one side of the plate, and water evaporates on the other. Plate evaporators can be manufactured using metal, plastic or polymer-coated metal. These plate heat exchangers have lower hold-up volumes, closer temperature approaches, lighter weights, smaller space requirements, higher heat transfer coefficients and lower fouling resistances. Irrespective of the many attractive features of plate evaporators they remain limited to experimental and prototype units [3].

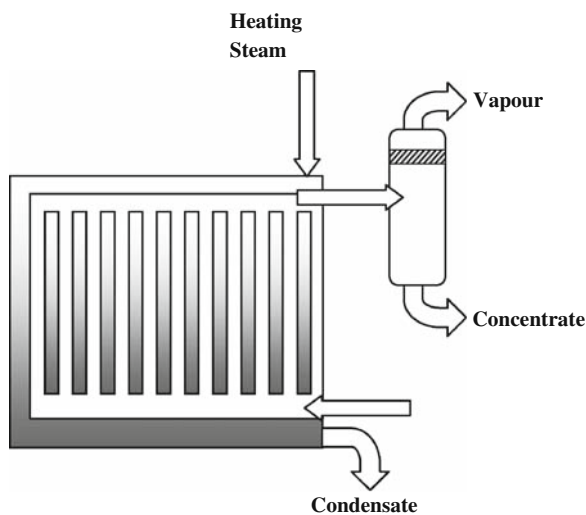


Fig. 2.4 Plate evaporator

2.3 Single-Effect Evaporation

The single-effect evaporation system for seawater desalination has no practical use on an industrial scale. This is because the system has a thermal performance ratio of less than 1, i.e. the mass of water produced is less than the mass of heating steam used to operate the system. However, the understanding of this process is essential as it is a constituent of other single-effect vapour compression systems, as well as multiple-effect evaporation processes [2].

Figure 2.5 shows a schematic diagram for a horizontal tube, falling film, single-effect evaporation system. The main components of the unit are the evaporator, feed preheater or down condenser, the vacuum system and the pumping units. As shown, the intake seawater ($M_{cw}+M_f$), at temperature T_{cw} and with salt concentration X_f , is introduced into the tube side of the preheater, where its temperature increases to T_f . The cooling water (M_{cw}) is released back into the sea. The function of the cooling water in the condenser is to remove excess heat added in the evaporator by the heating steam. This implies that the evaporator does not consume all the supplied heat, instead, it degrades its quality. The heating of the feed seawater (M_f) in the condenser tubes from T_{cw} to T_f is essential to increase the thermal performance of

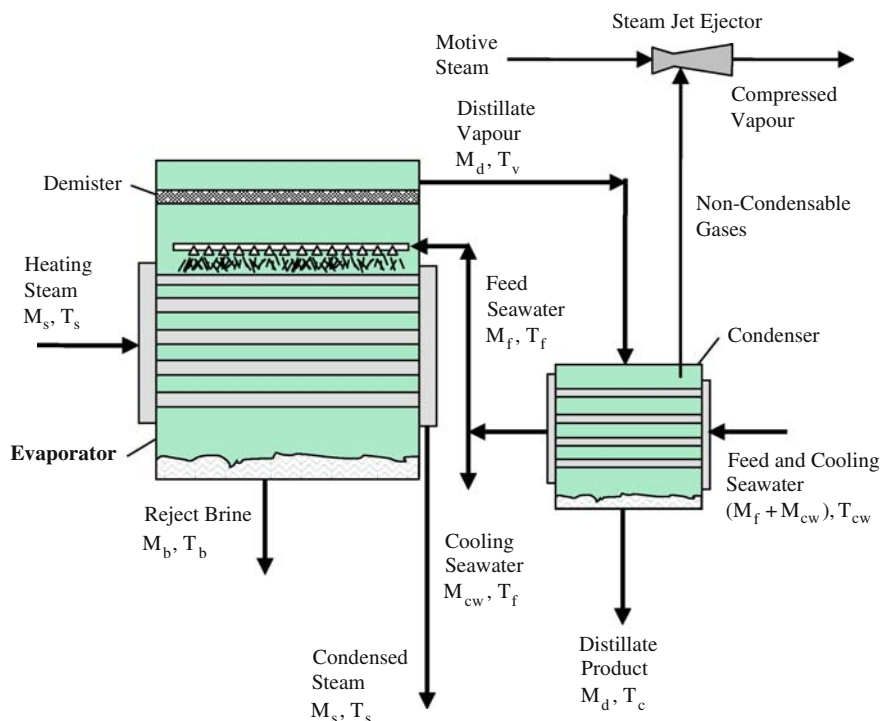


Fig. 2.5 Single-effect evaporation desalination process

the process. The heat needed to warm the seawater inside the condenser tubes is supplied by condensing the vapour formed in the evaporator (M_d).

The vapour condensation temperature and consequently the pressure in the vapour space, for both the evaporator and the condenser, is controlled by the cooling water flow rate (M_{cw}), the feed water temperature (T_{cw}), the available heat transfer area in the condenser (A_c), the overall heat transfer coefficient between the condensing vapour and the circulating seawater (U_c). Accordingly, the condenser has three functions: (1) to remove the excess heat from the system, (2) to improve the process performance ratio, and (3) to adjust the boiling temperature inside the evaporator.

The feed seawater (M_f) is chemically treated and de-aerated before being pumped into the evaporator. This chemical treatment is needed to prevent foaming and the tendency of scale formation in the evaporator. Both factors may seriously impair unit operation. Once inside the evaporator, the feed water is sprayed from the top; it falls in the form of a thin film through the rows of tubes arranged horizontally below. Condensation of the saturated heating steam, and release of its latent heat, provides the required sensible and latent heat for water evaporation from the feed seawater. As a result, the feed water temperature (T_f) is raised to boiling temperature (T_b). The value of T_b is mainly dictated by the type of chemicals used to control scale formation and the state of the heating steam. The vapour formed by boiling, with a flow rate of M_d , is completely free of salt. Figure 2.6 shows that the temperature of the generated vapour (T_v) is less than boiling temperature due to boiling-point elevation (BPE). Similarly, the temperature of the condensed vapour (T_d) is lower than the temperature of the generated vapour due to heat losses caused by the demister, transmission lines and condensation.

The generated vapour flows through a knitted wire mist separator, known as the wire mesh demister, to remove the entrained brine droplets. The vapour needs to be completely free of brine droplets to prevent contamination of the product water. This also prevents exposure of the condenser tubes to brine, which can result in scaling, surface corrosion and reduction of heat transfer rates. In thermal vapour compression, the presence of entrained water droplets in the vapour flowing into the steam jet ejector can result in erosion of the ejector nozzle and diffuser. The saturation temperature of the vapour leaving the demister is lower than (T_v). This temperature

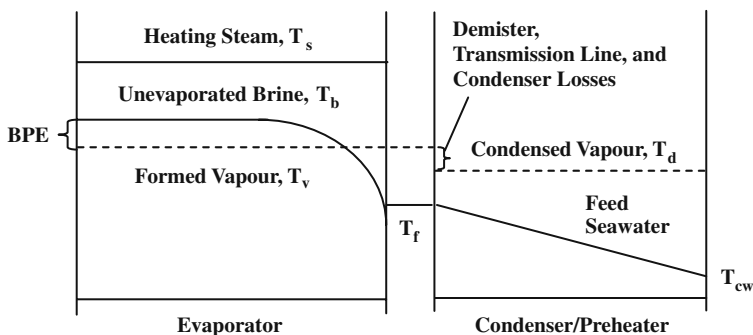


Fig. 2.6 Temperature profiles in evaporator and condenser of the single-effect evaporation system

reduction is caused by the frictional pressure loss in the demister. Further drops in pressure take place during vapour transfer between the evaporator and pre-heater and during vapour condensation. This further decreases the vapour condensation temperature.

The non-condensable gases in the vapour space of the condenser must be continuously vented to avoid downgrading of the heat transfer capacity of the condenser. The blanket of non-condensable gases masks some of the heat transfer area from the condensing vapour. In addition, the non-condensable gases reduce the partial pressure of the condensing vapours. As a result, condensation takes place at a lower temperature. This reduces process efficiency because of the decrease in the net driving force for heat transfer (i.e. the temperature difference between the condensing vapour and the stream, M_f), and consequently reduces the feed seawater temperature (T_f). Removal of these gases is made at points in the system where the temperature approaches its lowest value (i.e. that of cooling water entering the tubes). This permits the cooling of the non-condensable gases to the minimum possible temperature, thereby minimising the amount of vapour which escapes with the gases and decreasing the volume of pumped gases. In addition, it is possible to operate a counter-current condenser so that the exit water is within 3–5°C of the condensation temperature of the saturated vapour. This improves the thermal performance of the unit and minimises the mass flow rate of the cooling water.

2.3.1 Modelling of the Single-Effect Evaporator

Modelling and analysis of the evaporator can be based on a detailed set of equations that utilise a number of correlations to determine the heat transfer coefficient, thermodynamic losses, and physical properties of water and vapour. Solution of the detailed model requires an iterative procedure because of the non-linearity of the model equations and correlations. The model can be simplified by assuming constant physical properties, negligible heat losses to the surroundings, constant thermodynamic losses and a constant overall heat transfer coefficient. This assumption reduces the model to a set of material and energy balance equations, which can be used for design or simulation [6]. The evaporator energy balance is:

$$M_s \lambda_s = M_d \lambda_v + M_f C_p (T_b - T_f) \quad (2.1)$$

The left side of the equation defines the thermal load of the heating steam and the right hand side gives the latent heat of the formed vapour and the sensible heat of the feed seawater. The thermal load of the heating steam is also used to determine the required heat transfer area of the evaporator. This relationship is illustrated by:

$$A_e = \frac{M_s \lambda_s}{U_e (T_s - T_b)} \quad (2.2)$$

A similar set of equations can also be defined for the condenser and includes the condenser energy balance and the heat transfer equations:

$$M_d \lambda_d = (M_{cw} + M_f) C_p (T_f - T_{cw}) \quad (2.3)$$

$$A_c = \frac{M_d \lambda_d}{U_c \text{LMTD}_c} \quad (2.4)$$

In Eq. (2.4), the logarithmic mean temperature difference (LMTD_c) is given by the following relation:

$$\text{LMTD}_c = (T_{cw} - T_f) / \ln((T_d - T_f) / (T_d - T_{cw})) \quad (2.5)$$

Where it is worth noting that the distillate temperature T_d is lower than the brine temperature due to thermodynamic losses. The remaining model equations define the overall mass balance and the salt mass balance of the entire system:

$$M_f = M_d + M_b \quad (2.6)$$

$$X_f M_f = X_b M_b \quad (2.7)$$

Other important design aspects include the tube wetting rate, the velocity of the vapour inside the evaporator tubes and the water velocity inside the condenser tubes [7]. The tube wetting rate (WR) is defined as the feed flow rate per unit length of the top row of the tubes. This relationship is defined by:

$$\text{WR} = M_f / (n_{rt} L_t) \quad (2.8)$$

where n_{rt} is the number of tube rows, and L_t is the tube length.

The wetting rate should remain within a range of 0.03–0.14 kg/(m s); lower values result in formation of dry spots and higher values affect the thermal characteristics of the system. The vapour velocity inside the evaporator tubes is given by:

$$V_s = \frac{M_s \cdot v_s}{n_e \cdot \frac{\pi d_e^2}{4}} \quad (2.9)$$

where v_s is the steam specific volume, n_e is the total number of tubes in the evaporator and d_e is the tube diameter.

The vapour velocity may vary within a range of 20–50 m/s. A similar relationship is used to determine the water velocity inside the condenser tubes:

$$V_f = \frac{(M_f + M_{cw})}{\rho_{cw} \cdot n_c \cdot \frac{\pi d_c^2}{4}} \quad (2.10)$$

where ρ_{cw} is the cooling water density, n_c is the total number of tubes in the condenser and d_c is the tube diameter. The water velocity may vary within a range of 1–3 m/s. Lower velocities can result in increased rates of fouling and scaling

because of the increase in the contact time between the water and the tube wall. The upper limit on water velocity is set by the capacity of the feed pumps.

2.4 Multiple-Effect Distillation (MED)

The multiple-effect distillation process can be found in various industries, i.e. sugar, paper and pulp, dairy, textiles, acids and desalination. Small MED plants with capacities of less than 500 m³/day were introduced to the desalination industry in the 1960 s. Subsequent developments lead to the increase in unit production capacity. In 2006, MED capacity increased to a value of 36,000 m³/day [1]. Most MED processes operate at low temperatures, of less than 70°C. This is because the evaporators adopt a horizontal film configuration, where the feed seawater is sprayed on the outside surface of the tubes. Therefore low temperature operation limits the rate of scale formation on the outside surface of the evaporator tubes. Moreover, operation at low temperatures allows for efficient combination with thermal or mechanical vapour compression. The vapour compression process has been developed to improve the process performance ratio (kg product/kg heating steam) to values close to 16 for a twelve-effect system. The performance ratio drops to a value of 8 if the system operates with no vapour compression [8]. Prototype units of MED, combined with lithium bromide absorption vapour compression, give a performance ratio of more than 20 [9]. On a commercial scale, most MED systems are designed to operate in either standalone mode or in combination with thermal vapour compressors (MED/TVC). Mechanical vapour compression systems (MED/MVC) are found on a much more limited scale.

Ophir and Lokiec [10] presented a recent evaluation of the MED process and how its economics are superior to other desalination processes. As mentioned before, low temperature operation allows for highly efficient thermal vapour compression. It also allows for use of low grade energy. Another advantage is the use of relatively inexpensive construction material, which includes aluminium alloys for the heat transfer tubes, as well as carbon steel epoxy coated shells, for the evaporator shells. Ophir and Lokiec [10] reported water cost of \$0.54/m³ for a plant of 5 units, each producing 20,000 m³/day.

2.4.1 MED Process Description

Industrial MED systems include up to 12 evaporation effects, where evaporation in the first effect is driven by heat steam extracted from cogeneration boilers. The vapour formed in the first effect is used to drive evaporation in the second effect. This process continues in subsequent effects until the vapour temperature drops to about 30–40°C. Most industrial MED systems are designed to operate in dual mode, i.e. standalone, where it is driven by heating steam from the boiler, or in a thermal vapour compression mode, where part of the vapour formed in the last

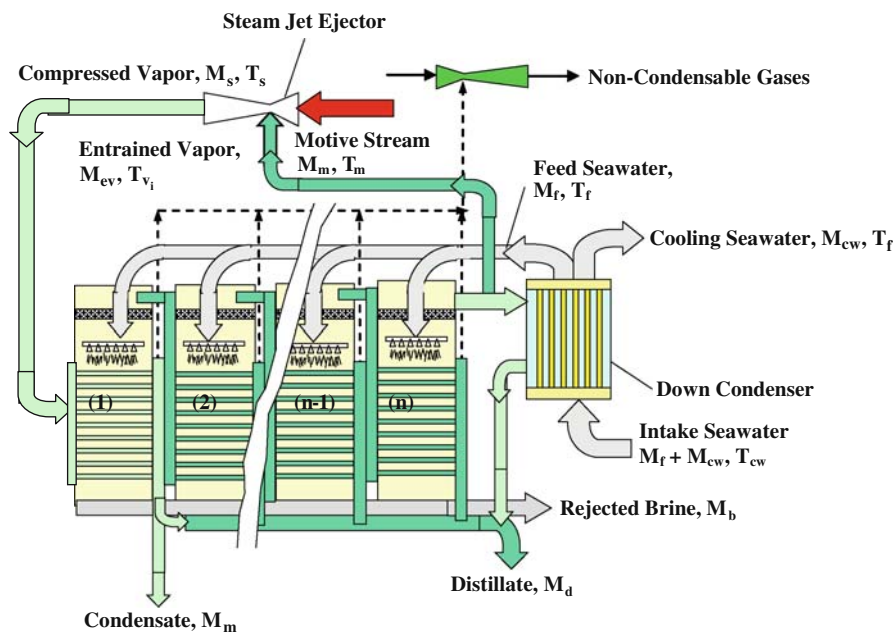


Fig. 2.7 Schematic of MED/TVC with thermal vapour compression

effect is compressed to the desired temperature and used to drive evaporation in the first effect. Figure 2.7 shows a schematic for a thermal vapour compression system (MED/TVC).

A small proportion of the MED system utilises a mechanical vapour compression configuration, where the entire vapour formed in the last effect is compressed mechanically to the desired temperature, and is used to drive evaporation in the first effect. Limitations in the compression capacity of the mechanical vapour compressor limit the number of effects in the system to less than 6.

Figure 2.8 shows a schematic for an MED/MVC process. MED/MVC systems, as shown in Fig. 2.8, have similar layouts to thermal vapour compression processes. The main differences are the absence of a down condenser and the use of a mechanical compressor, to compress the entire vapour formed in the last effect to the desired heating steam temperature. In addition, the outlet brine and distillate streams exchange heat with the feed stream in two pre-heaters.

2.4.2 Modelling and Design of MED and Vapour Compression

The MED model is based on the same set of equations used to model the single-effect evaporation process. The following analysis utilises the detailed model, which includes detailed correlations for heat transfer coefficients, physical properties and thermodynamic losses [7]. The model is used to design 30,000 m³/day MED and

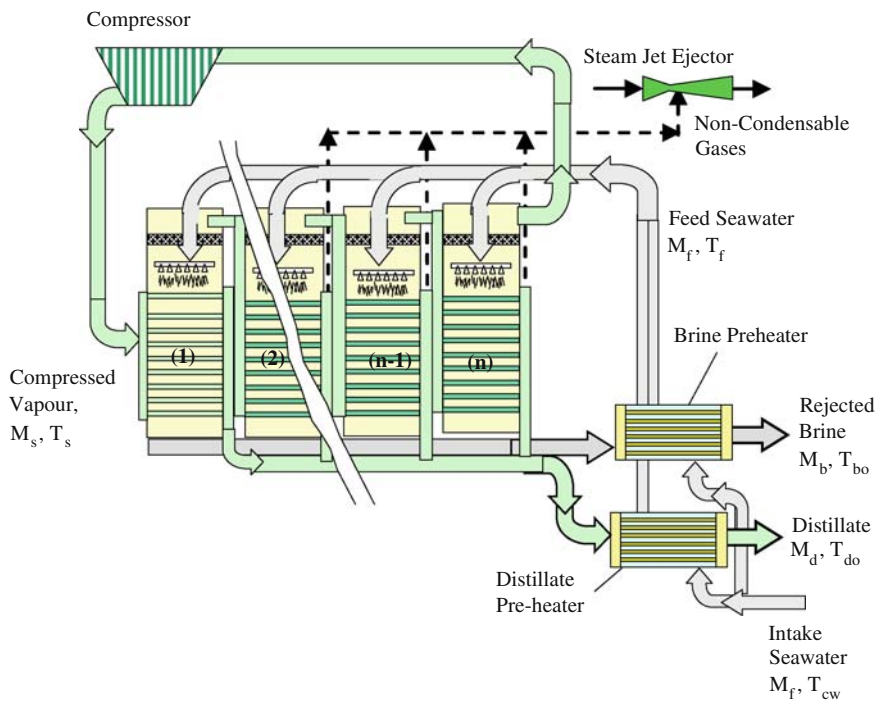


Fig. 2.8 Schematic of MED/MVC with mechanical vapour compression

MED/TVC systems. The calculations are performed for 8, 10, and 12 effects and heating steam temperatures of 65, 70 and 75°C. The system performance ratios and specific heat transfer areas are shown in Figs. 2.9 and 2.10, respectively.

Figure 2.9 shows the increase in performance ratio as the number of effects increases. This is caused by the constant production capacity used in all configurations, which results in a reduction in the amount of vapour formed in each effect, as the number of effects is increased. Therefore, the amount of heating steam required to drive evaporation in the first, reduces with the amount of vapour formed in each effect.

Figure 2.10 shows that the specific heat transfer area increases with the increase in the number of effects, and decreases with the increase in heating steam temperature. The increase in the specific heat transfer area, with the increase in the number of effects, is caused by a reduction in the temperature drop from one effect to the next, which reduces the driving force for heat transfer. This is because the temperature difference between the first and last effect is kept constant in all calculations. Increasing the heating steam temperature reduces the specific heat transfer area as the brine blow down temperature is kept constant in all calculations. Therefore the temperature drop from one effect to the next increases and results in an increase in the driving force for heat transfer in each effect.

Fig. 2.9 Variations in performance ratio as a function of heating steam temperature and number of effects

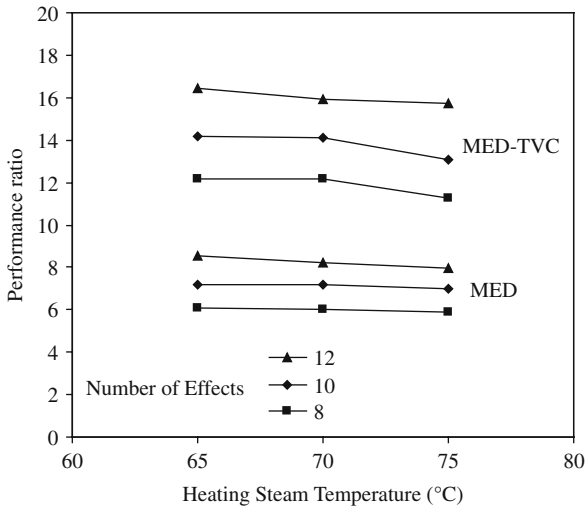
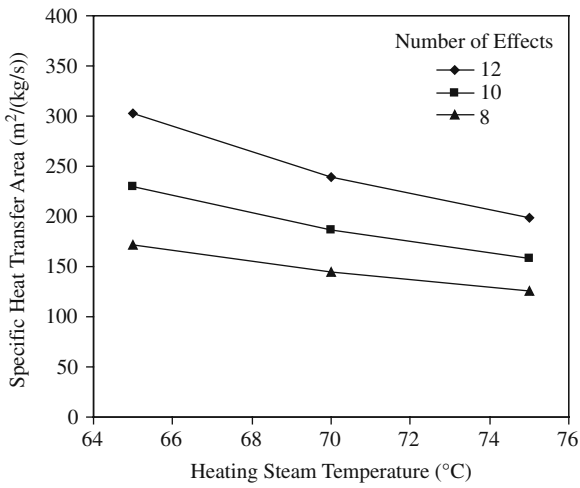


Fig. 2.10 Variations in specific heat transfer area as a function of heating steam temperature and number of effects



2.5 Single-Effect Mechanical Vapour Compression (MVC)

The MVC system was introduced in the 1980 s. Early studies by Matz and Fisher [11], Lucas and Tabourier [12] and Matz and Zimerman [13] were motivated by the need to develop a thermal desalination process driven solely by electrical power. The MVC process was pursued as a competitor to the newly introduced RO technology. However, the test of time has shown the dominance of the RO process and a very limited growth in the reliability of MSF and MED processes.

MVC unit capacity is very small in comparison with MSF and MED. Current unit capacity is below $5,000 \text{ m}^3/\text{day}$. However, recent conceptual designs by Kronenberg and Lokiec [14] demonstrate the feasibility of constructing units with $10,000 \text{ m}^3/\text{day}$ capacity. The small size, and the fact that only electrical power is required, makes it feasible to operate using various forms of renewable energy, i.e. wind, photovoltaics, etc. On average MVC consumes $10\text{--}14 \text{ kWh/m}^3$ of electrical power, to operate the system and other associated equipment including pumps, controls and auxiliaries. A $5,000 \text{ m}^3/\text{day}$ MVC would thus require $2\text{--}3 \text{ MW}$ of electrical power, which can be easily provided by available renewable energy technologies.

2.5.1 Description of the MVC Process

Schematics for an MVC process are shown in Figs. 2.11 and 2.12. As shown in Fig. 2.11, the system contains a horizontal tube evaporator, spray nozzles, a vapour compressor, a recycle pump and plate preheaters. A cross section of the tube arrangement, spray nozzles, demister and compressor intake are shown in Fig. 2.12. As shown in Fig. 2.11, the heating steam or compressed vapour flows within the tubes and the brine is sprayed on the outside surface of the tubes. To limit the rate of scale formation on the outside surface of the tubes, the maximum possible saturation temperature of the compressed vapour is 70°C . As shown in Fig. 2.12, the tube bank is divided into two groups on either sides of the demister, which is placed in

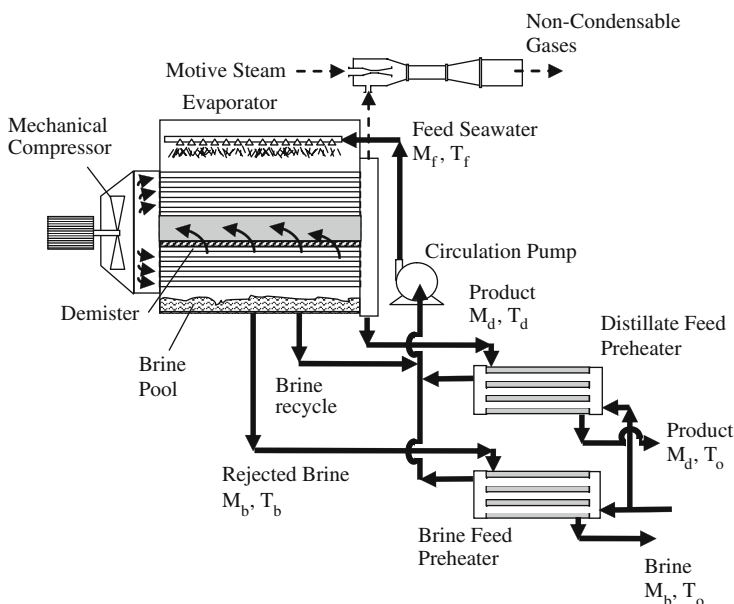
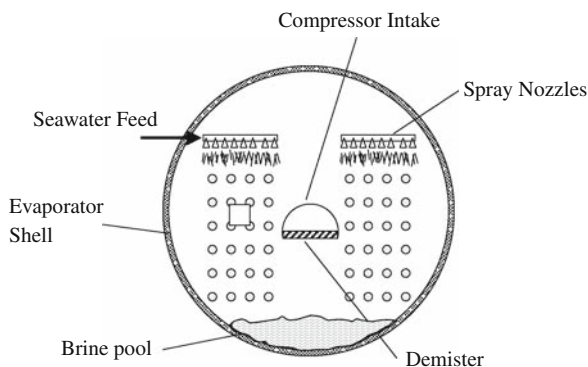


Fig. 2.11 Single-effect mechanical vapour compression

Fig. 2.12 Cross section of the evaporator showing two tube banks with square pitch, spray nozzles, demister, compressor intake and brine pool



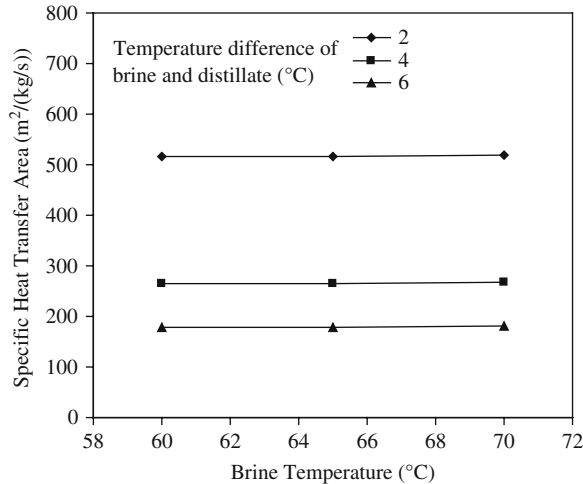
the centre of the evaporator. The demister arrangement is connected directly to the compressor intake, where the formed vapour is compressed and superheated to the desired temperature. The feed water entering the system is pre-heated in two plate exchangers using the distillate condensate and the brine reject. Plate preheaters are compact and allow for a small approach temperature. Brine circulation takes place within the evaporator to achieve the desired wetting rate, i.e. the mass of sprayed water per unit length of top row tubes should be within a range of 0.03–0.14 kg/(m s). This is necessary to prevent formation of dry spots or flooding within the system [15]. Accumulation of non-condensable gases within the evaporator is controlled by the use of a jet ejector. Pumping units used in the system include pumps for the feed, distillate, brine reject and brine recycle.

2.5.2 Modelling and Design of MVC

MVC modelling focuses on the determination of the required heat transfer area for the evaporator and feed preheaters, power capacity of the compressor, brine circulation flow rate, tube arrangement, shell diameter, pumping power and capacity of the venting system. Commonly used assumptions in model development are: steady state conditions, distillate is salt-free, negligible heat losses to the surroundings and negligible vapour losses in the venting line [16]. Details of the model equations, correlations and solution method can be found in various studies by Darwish [17], El-Dessouky and Ettouney [2], Ettouney [16], Ettouney et al. [7].

The performance of MVC is illustrated in terms of variations in the specific heat transfer area and the specific power consumption, and as a function of brine temperature and the temperature difference between distillate condensate and brine (Figs. 2.13 and 2.14). As shown in Fig. 2.13, the specific heat transfer area has a negligible dependence on brine temperature. This effect is caused by the limited variation in the overall heat transfer coefficient that occurs upon varying the brine temperature. However, an increase in the temperature difference between the distil-

Fig. 2.13 Variations in specific heat transfer area of the MVC system as a function of brine temperature and the temperature difference between distillate brine



late and brine stream considerably reduces the heat transfer area. This is because of the increase in the driving force for heat transfer between the condensed vapour and the evaporating brine.

Variations in the specific power consumption for the system are shown in Fig. 2.14. The specific power consumption has little dependence on brine temperature, where the specific power consumption decreases with increases in brine temperature. This is caused by the decrease in the specific volume of the intake vapour, which in turn reduces the required compression power. The specific power consumption has a much greater dependence, however, on the temperature difference between distillate and brine. This is caused by the increase in the compression ratio of the vapour.

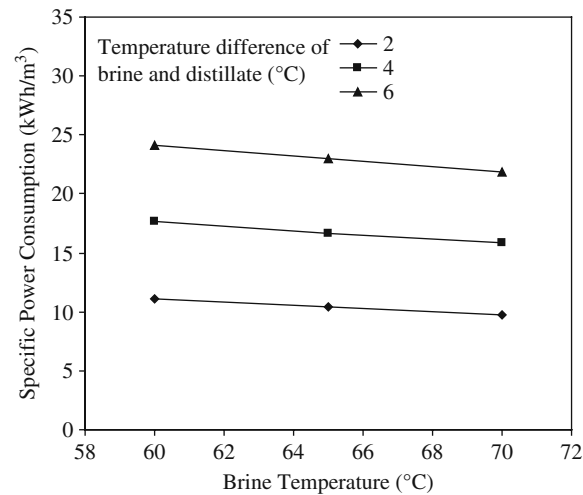


Fig. 2.14 Variations in specific power consumption for the MVC system, as a function of brine temperature and temperature difference between distillate and brine

A review of the data shown in Figs. 2.13 and 2.14 shows the need to optimise the temperature difference between brine and distillate. Operation at small differentials would result in large heat transfer areas; on the other hand, increases in the temperature differentials cause large increases in specific power consumption. The heat transfer area and the consumed power have significant effects on the product cost.

2.6 Multi-Stage Flash Desalination (MSF)

The MSF desalination process was introduced in the early 1950 s. In 1957, Silver patented the multi-stage flash desalination process [18]. The patent optimised the number of flashing stages and the heat transfer area. Since then, the MSF process has gone through several dramatic modifications and improvements, which have lead to a massive increase in unit capacity, from 500 m³/day in the 1960 s to 75,000 m³/day in the 1990 s [19]. Other developments include the use of demisters in all flashing stages, which limits entrainment rates of brine by the flashed-off vapour. As a result, product salinity is maintained below 10 ppm. Also, development of the on-line ball cleaning system has resulted in less frequent use of acid cleaning and plant shutdown. Currently, MSF plants can be operated for periods varying from 2 to 5 years before a major overhaul is necessary [20]. Recent field experience shows that a large number of old MSF plants are being rehabilitated to improve performance and extend service life [21, 22].

2.6.1 MSF Flashing Chamber

The main element in the MSF process is the flashing chamber. A schematic of the MSF flashing stage is shown in Fig. 2.15 and includes the following items.

A large brine pool with a similar width and length to the flashing stage and with a depth of 0.2–0.5 m.

A brine transfer device, comprising a weir and splash plate combination between the stages, is designed to seal the vapour space between the stages and to enhance turbulence and mixing of the inlet brine stream. This device promotes flashing by controlling the formation of vapour bubbles, their growth and subsequent release.

A demister formed of wire mesh layers and supporting system. The demister function is to remove the entrained brine droplets from the flashed-off vapour. This is essential to prevent an increase in the salinity of the product water and scale formation on the outer surface of the condenser tubes.

A tube bundle of condenser/pre-heater tubes, where the flashed-off vapour condenses on the outer surface of the tubes. The released latent heat of condensation results in heating of the brine recycle stream flowing inside the tubes. This energy recovery is essential to maintain high system performance.

A distillate tray, where the condensed distillate product is collected and cascades through the stages. The distillate product is withdrawn from the tray in the last stage.

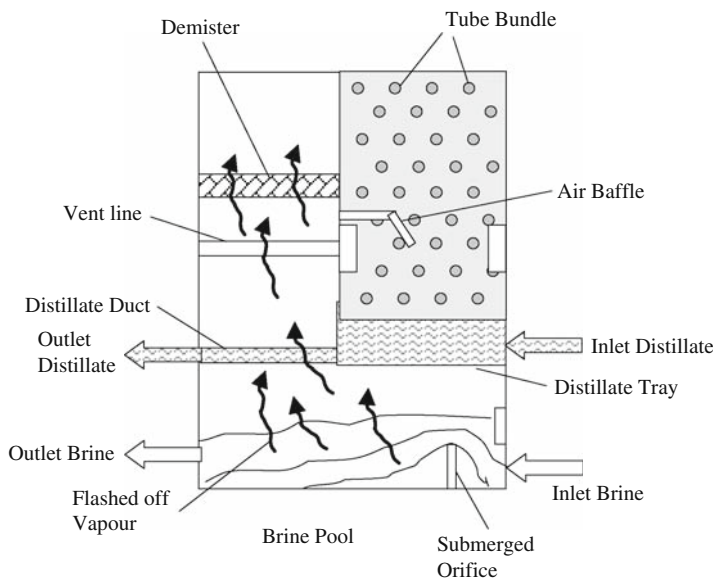


Fig. 2.15 MSF flashing stage

Water boxes at both ends of the tube bundle to transfer the brine recycle stream between adjacent stages.

Connections for the venting system, which remove non-condensable gases (O_2 , N_2 and CO_2), which are dissolved in the feed seawater, even after de-aeration. CO_2 can also be generated during decomposition of bicarbonate compounds in the high temperature stages. Another major source of non-condensable gases is air in-leakage from the ambient surroundings into flashing stages operating at temperatures below $100^\circ C$, which correspond to vacuum conditions.

Instrumentation, which includes thermocouples, a level sensor and a conductivity meter, is placed in the first and last flashing stages. The data measured at these stages is used by the process control system. Accordingly, and subject to disturbances in the system parameters, i.e. feed seawater temperature, increase in fouling thermal resistance, available steam, etc., adjustments are made in the controllers to maintain the desired operating conditions. The magnitude of these adjustments depends on the measurements made in the first and last stages.

2.6.2 MSF Processes

There are two main layouts for the MSF process. The first is the once-through system and the second is the brine circulation system. The brine circulation system is to be found on a larger scale than the once-through system. Figure 2.16 shows a schematic for the MSF once-through process. As shown, the system includes brine heater, flashing stages, vacuum ejector, chemical addition pumps and feed screens [23].

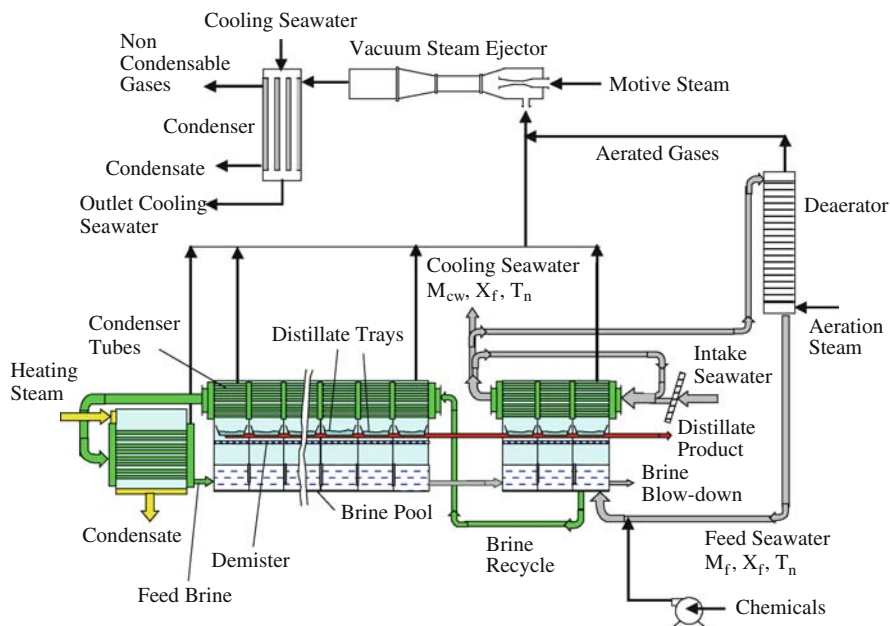


Fig. 2.17 Brine circulation multi-stage flash process

of the specific volume of the flashed-off vapour and a subsequent increase in vapour velocity, as well as an increase in the amount of entrained brine. This in turn would cause an increase in product salinity and the product stream might not be suitable for use as makeup boiler water. Instead, part of the distillate product in the first stages should be used.

De-aeration of the feed seawater is an essential element in the MSF brine circulation system. It removes dissolved gases from the feed stream, i.e. oxygen, nitrogen, and carbon dioxide. If these gases are not removed, they will be released in the flashing stages. The released gases have low thermal conductivity and would reduce the heat transfer rate around the condenser tubes. Carbon dioxide and oxygen may also promote corrosion reactions in various locations in the flashing stages. The de-aerator may have a vertical or horizontal configuration equipped with spray nozzles or trays. De-aeration is performed by heating steam, which results in an increase in the feed temperature and as a result reduces gas solubility in the feed water.

2.6.3 Modelling and Design of MSF

The MSF model assumptions are similar to those for the MVC and MED systems. The system model can be simplified or made more complex depending on the assumptions used to define the heat transfer coefficient, thermodynamic losses and physical properties. Basic model equations have been developed to describe the material and energy balance in each flashing stage.

These equations include:

- global mass balance,
- salt mass balance
- energy balance for the flashing brine,
- energy balance for the condenser tubes,
- heat transfer equation for the condenser tubes.

They can be described as follows:

$$B_{j-1} = B_j + D_j \quad (2.11)$$

$$X_{b_{j-1}} \cdot B_{j-1} = X_{b_j} \cdot B_j \quad (2.12)$$

$$D_j \cdot \lambda_j = B_{j-1} \cdot C_{pbj} \cdot (T_{b_{j-1}} - T_{b_j}) \quad (2.13)$$

$$D_j \cdot \lambda_{c,j} + C_{pd} \cdot (T_{c_{j-1}} - T_{c_j}) \sum_{k=1}^{j-1} D_k = M_f \cdot C_{pfj} \cdot (T_{f_j} - T_{f_{j+1}}) \quad (2.14)$$

$$M_f \cdot C_{pfj} \cdot (T_{f_j} - T_{f_{j+1}}) = U_{c_j} \cdot A_c \cdot (LMTD)_{c_j} \quad (2.15)$$

Other model equations for the brine heater, which include energy balance and heat transfer equations, are as follows:

$$M_s \cdot \lambda_s = U_h \cdot A_h \cdot (LMTD)_h \quad (2.16)$$

$$(LMTD)_h = \frac{(T_s - T_{b_0}) - (T_s - T_{f_1})}{\ln \left(\frac{(T_s - T_{b_0})}{(T_s - T_{f_1})} \right)} = \frac{(T_{f_1} - T_{b_0})}{\ln \left(\frac{(T_s - T_{b_0})}{(T_s - T_{f_1})} \right)} \quad (2.17)$$

$$M_s \cdot \lambda_s = M_f \cdot C_{ph} \cdot (T_{b_0} - T_{f_1}) \quad (2.18)$$

Further model details can be found in studies by Abdel-Jabbar, et al. [24], El-Dessouky and Ettouney [2], and Ettouney et al. [23]. These studies give variations in the system performance ratio, specific heat transfer area, and the specific flow rates of cooling water and brine recycle. The analysis is performed as a function of maximum brine temperature (temperature of brine entering the first stage), or Top Brine Temperature (TBT), and number of stages.

The design and analysis presented here is limited to variations in the specific heat transfer area as a function of system production capacity and maximum brine temperature. Additional design data and performance analysis can be found in the studies which have been previously cited. These studies include evaluation of variations in the system performance ratio and specific flow rates of the cooling seawater and brine recycle, as well as stage dimensions. In addition, there are other models and

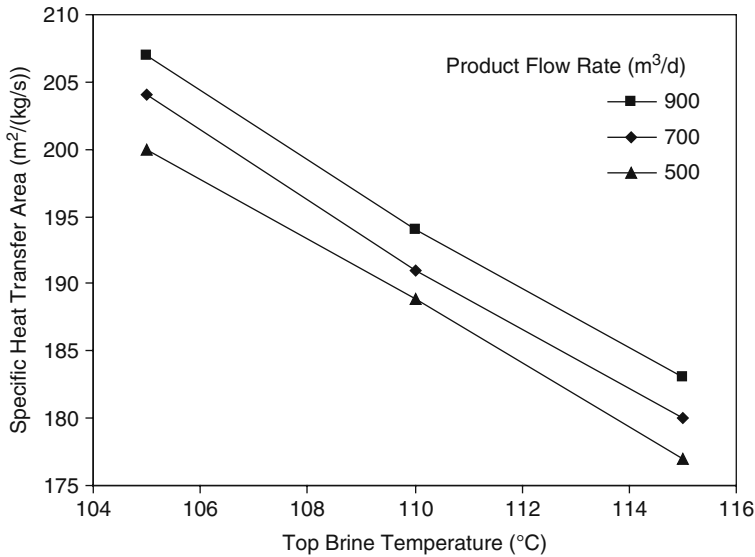


Fig. 2.18 Variations in specific heat transfer area as a function of top brine temperature and product flow rate

analyses which focus on thermo-economic optimisation [25, 26], system dynamics [27] and control [28].

Variations in the specific heat transfer area are shown in Fig. 2.18. As shown, the specific heat transfer area decreases with increase in the maximum brine temperature. This is because of the increase in flashing range and the temperature drop between one stage and the next, which increases the driving force for heat transfer. Also, the specific heat transfer area increases with the increase in production capacity. This is due to the increase in the thermal load of the system.

Nomenclature

A	Heat transfer surface area, m ²
B	Brine flow rate, kg/s
C _p	Specific heat at constant pressure, kJ/kg °C
d	Diameter, m.
D	Flow rate of distillate formed by evaporation, in the <i>i</i> th effect, kg/s
L	Length, width or thickness, m
LMTD	Logarithmic mean temperature difference, °C
M	Mass flow rate, kg/s
n	Number of tubes
T	Temperature, °C
U	Overall heat transfer coefficient, kW/m ² °C

v	Specific volume, m ³ /kg
V	Velocity, m/s
WR	Wetting rate, kg/(m s)
X	Salinity, ppm

Greek Symbols

λ	Latent heat of vaporization, kJ/kg
ρ	Density, kg/m ³

Subscripts

b	Brine
c	Condenser or condensate
cw	Cooling water or intake seawater
d	Distillate
e	Evaporator
f	Feed seawater
h	Brine heater
j	jth stage
o	Brine leaving the brine heater
rt	Number of tube rows
s	Heating steam
t	tube
v	Saturated vapour

Abbreviations

IDA	International Desalination Association
LMTD	Logarithmic Mean Temperature Difference
MED	Multiple-Effect Distillation
MSF	Multi-stage Flash
MVC	Mechanical Vapour Compression
TBT	Top Brine Temperature
TVC	Thermal Vapour Compression

References

1. IDA, Int. Desalination Association, Worldwide Desalting Plants Inventory, 2006.
2. El-Dessouky, H.T., and Ettouney, H.M., Fundamentals of Salt Water Desalination, Elsevier, New York, USA, 2002.

3. Tonner, J.B., Hinge, S., and Legorreta, C., Plates – the next breakthrough in thermal desalination, *Desalination*, 134 (2001) 205–211.
4. Yang, L., and Shen, S., Experimental study of falling film evaporation heat transfer outside horizontal tubes, *Desalination*, 220 (2008) 654–660.
5. Renaudin, V., Kafi, F., Alonso, D., and Andreoli, A., Performances of a three-effect plate desalination process, *Desalination*, 182 (2005) 165–173.
6. El-Dessouky, H.T., Alatiqi, I., and Ettouney, H.M., Process synthesis: The multi-stage flash desalination system, *Desalination*, 115(1998) 155–179.
7. Ettouney, H.M., Abdel-Jabbar, N., Mjalli, F.S., and Qiblawy, H., Development of Web Based Computer Package for Simulation of Thermal and Membrane Desalination Processes, final report, Project ID MEDRC-04-AS-001, MEDRC, Muscat, Oman, 2008.
8. Temstet, C., Canton, G., Laborie, J., and Durante, A., A large high-performance MED plant in Sicily, *Desalination*, 105 (1996) 109–114.
9. de Gunzbourg, J., and Larger, D., Cogeneration applied to very high efficiency thermal seawater desalination plants, *Desalination* 125 (1999) 203–208.
10. Ophir, A., and Lokiec, F. Advanced MED process for most economical sea water Desalination, *Desalination* 182 (2005) 181–192.
11. Matz, R., and Fisher, U., A comparison of the relative economics of sea water desalination by vapor compression and reverse osmosis for small to medium capacity plants, *Desalination*, 36 (1981) 137–151.
12. Lucas, M., and Tabourier, B., The mechanical vapour compression process applied to seawater desalination: a 1500 ton/day unit installed in the Nuclear Power Plant of Flamanville, France, *Desalination*, 52 (1985) 123–133.
13. Matz, R., and Zimmerman, Z., Low-temperature vapour compression and multi-effect distillation of seawater. Effects of design on operation and economics. *Desalination*, 52 (1985) 201–216.
14. Kronenberg, G., and Lokiec, F., Low-temperature distillation processes in single- and dual-purpose plants, *Desalination*, 136 (2001) 189–197.
15. Han, J., and Fletcher, L., Falling film evaporation and boiling in circumferential and axial grooves on horizontal tubes, *Ind. Eng. Chem. Process Des. Dev.*, 24 (1985) 570–597.
16. Ettouney, H.M., Design of single effect mechanical vapor compression, *Desalination*, 190 (2006) 1–15.
17. Darwish, M.A., Thermal analysis of vapor compression desalination system, *Desalination*, 69 (1988) 275–295.
18. Silver, R.S., Multi-stage flash distillation – the first 10 years, 3rd Int. Sym. On Fresh Water from the Sea, Athens, Greece, 1 (1970) 191–206.
19. Borsani, R., and Rebagliati, S., Fundamentals and costing of MSF desalination plants and comparison with other technologies, *Desalination* 182 (2005) 29–37.
20. Al-Falah, E., Al-Shuaib, A., Ettouney, H.M., and El-Dessouky, H.T., On-Site training program in desalination plants, *Eu. J. Eng. Edu.*, 26 (2001) 407–418.
21. Thirumeni, C., Deutsche Babcock Rehabilitation and uprating of Ras Abu Fontas MSF, desalination units: process optimisation and life extension, *Desalination* 182 (2005) 63–67.
22. Helal, A.M., Uprating of Umm Al Nar East 4-6 MSF desalination plants, *Desalination* 159 (2003) 43–60.
23. Ettouney, H.M., El-Dessouky, H.T., and Al-Juwayhel, F., Performance of the once through multistage flash desalination, *Proc. Inst. Mech. Eng. Part A, Power and Energy*, 216 (2002) 229–242.
24. Abdel-Jabbar, N.M., Qiblawey, H.M., Mjalli, F.S., and Ettouney, H., Simulation of Large Capacity MSF Brine Circulation Plants, *Desalination*, 204 (2007) 501–514.
25. Fiorini, P., and Sciubba, E., Thermoeconomic analysis of a MSF desalination plant, *Desalination*, 182 (2005) 39–51.
26. Cipollina, A., Micale, G., and Rizzuti, L., Investigation of flashing phenomena in MSF chambers, *Desalination*, 216 (2007) 183–195.

27. Bogle D., Cipollina A., and Micale G., Dynamic modelling tools for solar powered desalination processes during transient operations, in *Solar Desalination for the 21st Century* (Eds. L. Rizzuti, H.M. Ettouney, A. Cipollina), Springer. ISBN: 978-1-4020-5506-5 (2007).
28. Tarifa, E.E., Domínguez, S.F., Humana, D., Martínez, S.L., Nunez, A.F., and Scenna, N.J., Faults analysis for MSF plants, *Desalination*, 182 (2005) 131–142.

Seawater Desalination

Conventional and Renewable Energy Processes

Cipollina, A.; Micale, G.D.M.; Rizzuti, L. (Eds.)

2009, XIV, 306 p. 135 illus., Hardcover

ISBN: 978-3-642-01149-8